

Mitigation of Through-wall Interference in Radar Images Using Denoising Autoencoders

Shelly Vishwakarma, Vahini Ummalaneni, Muhammad Shoaib Iqbal, Angshul Majumdar and Shobha Sundar Ram
Indraprastha Institute of Information Technology Delhi
New Delhi, India 110020
{shellyv,vahini14169,mohd14148,angshul,shobha}@iiitd.ac.in

Abstract—The detection and identification of humans and concealed objects by through wall radars is affected by wall propagation effects such as attenuation and multipath. Several works, in the past, have provided solutions for mitigating wall effects based on either prior information of the wall parameters or signal processing solutions for separating wall interference from the direct signal from the target to the radar. In this paper, we propose a machine learning based method- denoising autoencoders- to mitigate wall interference effects and for reconstructing an image resembling the ground truth in free space conditions. This method relies on training the algorithm to denoise corrupted through-wall radar images into clean line-of-sight images. We have demonstrated the effectiveness of the proposed solution using simulated narrowband Doppler-Azimuth images in free space and through-wall conditions. We simulated the propagation through diverse wall conditions using stochastic finite difference time domain techniques. Next, we tested the algorithm on measured frontal (Azimuth-Elevation) images obtained from Walabot - a wideband, low power, radar with a planar antenna array. Both the measurement and simulation results showed a low error between the denoised reconstructed images and the clean line-of-sight images.

Index Terms—Through-wall radar, Doppler-DOA Imaging, sFDTD, Denoising Autoencoders

I. INTRODUCTION

Through-the-wall radars have been extensively researched and developed in the recent years for law enforcement, security and surveillance applications as well as search and rescue missions [1], [2]. The objective of the radar is usually to detect and track humans and other concealed objects or to infer building layouts [3]. The radars typically operate below X band frequencies to allow for the penetration of the electromagnetic signals through the wall materials. Both narrowband and broadband through-wall radars have been investigated. Usually the narrowband radars such as [4] and [5] have yielded Doppler based radar images while the broadband radars provide top-view images in range and cross-range. Both types of radars are, however, affected by through-wall propagation effects. We divide them into broadly two categories- First, multipath generated through reflections from the target to side and back walls resulting in ghost targets. Second reverberations within the front wall leading to de-focusing of targets in the radar images. Walls are complex mediums. While even single layer homogeneous walls can introduce attenuation, refraction and ringing to the propagating signal, in-homogeneous walls

such as brick and cinder block walls can result in significant distortions to the resulting radar signatures [6]. Therefore, there has been extensive research devoted to the mitigation of through-wall effects on the radar images [7], [8]. There have been two broad strategies towards tackling the problem - The first strategy relies on the availability of prior information regarding wall parameters such as the dielectric constant and the wall thickness. Then raw radar data are processed to correct for the wall effects [7]. The second strategy that is adopted involves the separation of the true target response from the interference introduced by the wall. This could be based on their distinct sparsity patterns [9] or their aspect dependent responses [8] or their images patterns or dictionaries [10] etc.

In this paper, we propose a third strategy for mitigating wall interference effects using denoising autoencoders [11]. Autoencoders are neural networks that employ unsupervised learning. They have been widely used for dimensionality reduction, denoising and representation learning applications. The main advantage of the proposed technique over the prior works is that the autoencoders require neither prior information regarding the wall characteristics nor any kind of analytic framework to describe the through-wall interference. Instead, the distorted radar images due to wall interference are treated as corrupt versions of ideal radar images obtained in free space conditions. The algorithm "learns" how to denoise or clean the corrupted images using training data comprising of both corrupted and clean data. As a result, the technique can be useful for removing the distortions introduced by very complex through-wall propagation effects. Conventional autoencoders have been implemented using back-projection algorithms such as gradient descent, steepest descent and conjugate gradient descent. In this work, we use an alternating direction method of multipliers (ADMM) [12]. The advantages are that we can break the complex convex optimization problem into smaller sub problems which already have closed form solutions. Hence the convergence is guaranteed. We test the performance of the algorithm on both simulated and measured radar data. We simulate narrowband Doppler radar data in free space and through-wall conditions. We consider interference introduced by three types of walls - a dielectric wall, a dielectric wall with metal reinforcements and a dielectric wall with airgaps. In each of these cases, we introduce substantial variation to the electric characteristics of the wall. We model the wall

diversity using the stochastic finite difference time domain (sFDTD) techniques as described in [13]. We generate the Doppler-azimuth radar images in free space and through-wall conditions and train the autoencoder to denoise the corrupted through-wall radar images to obtain the clean free space images. Our results show a very low normalized mean square error between the denoised images and free space images. For the measurement scenario, we use the Walabot, a wideband imaging radar for collecting frontal images both in free space and in through-wall conditions. Again we train the autoencoder to denoise the corrupted through-wall radar images to obtain clean radar images corresponding to the target in free space.

Our paper is organized as follows. In Section. II, we describe the autoencoder that we have implemented for our work. Then in Section. III, we describe the formulation of the stochastic FDTD used to generate narrowband Doppler-DOA radar images in both free space and through-wall conditions and results from the denoising algorithm are also presented here. In Section. IV, we describe the measurement set up used to collect wideband radar data (frontal images) using the Walabot imaging sensor in both free space and through-wall conditions along with the results of the denoising algorithm.

II. THEORY

In this section, we describe the denoising autoencoders used for mitigating the through-wall effects from both the simulation and the measured radar data. Autoencoders are neural networks used for unsupervised learning tasks such as dimensionality reduction and data denoising. The simplest form of an autoencoder is shown in Fig.1. It has one input layer $x \in \mathbb{R}^{d \times 1}$, one output layer $\tilde{x} \in \mathbb{R}^{d \times 1}$, and one or more hidden layers connecting the input and output. In the first stage of the autoencoder - the encoding stage - the algorithm tries to learn a latent/hidden layer representation $z \in \mathbb{R}^{r \times 1}$ of the input x , as shown in (1)

$$z = \phi(W_1 x) \quad (1)$$

Here, ϕ is an activation function which can be either sigmoid or rectified linear unit (ReLU) and W_1 is the corresponding weight matrix. In the second stage of the autoencoder - the decoding stage - the algorithm maps z back to obtain a reconstructed version of the input \tilde{x} using another weight matrix W_2 . Since the output layer of the autoencoder is a reconstructed version of the input, both have the same number of nodes. The hidden layer, on the other hand, has fewer nodes since it represents a compressed version of the input data.

$$\tilde{x} = W_2 z \quad (2)$$

The objective of the algorithm is to learn W_1 and W_2 such that the error e in (3) is minimized.

$$e = \|x - \tilde{x}\|_2^2 \quad (3)$$

The error, e , back propagates through the network and updates the weights in order to reduce the residual error using algorithms such as gradient descent, conjugate gradient descent or steepest descent. However, there are limitations

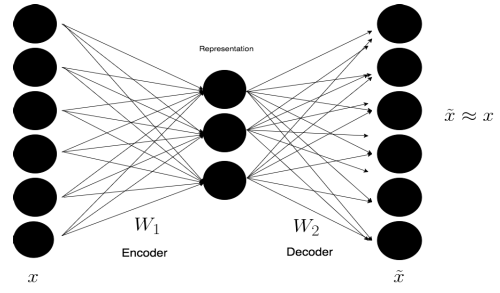


Fig. 1: Denoising Autoencoder.

associated with these algorithms - When the network consists of multiple layers, the error, at times, becomes insignificant before reaching the first layer. Also, these algorithms have a very slow learning rate. For denoising, autoencoder first corrupts the input data x by adding stochastic Gaussian noise, then feeds this corrupted version \hat{x} as an input. The error is still computed between the reconstructed signal \tilde{x} and the clean data x . In our case, due to the non-Gaussian nature of interference, we consider the measurements in through-wall case as the noisy/corrupted $\tilde{X} \in \mathbb{R}^{d \times n}$ data and the ones captured in free space as clean data $X \in \mathbb{R}^{d \times n}$. Here, columns of the data represent 'n' number of d-dimensional radar signal measurements. We reformulate the objective function of our denoising problem using (4). We use \tilde{X}^{tr} to train our network and \tilde{X}^{test} to test the denoising performance of our algorithm.

$$J(W_1, W_2) = \min_{W_1, W_2} \left\| X^{tr} - W_2 \phi(W_1 \tilde{X}^{tr}) \right\|_2^2 \quad (4)$$

Here, $W_1 \in \mathbb{R}^{r \times d}$ and $W_2 \in \mathbb{R}^{d \times r}$ are the weight matrices of the network and r defines the number of nodes in the hidden unit. We use a variable splitting technique to solve (4). Therefore, another proxy variable $Z = \phi(W_1 \tilde{X}^{tr})$ is defined such that the new objective function is expressed as (5).

$$J(W_1, W_2) = \min_{W_1, W_2} \|X^{tr} - W_2 Z\|_2^2 \quad (5) \\ \text{s.t. } Z = \phi(W_1 \tilde{X}^{tr})$$

We formulate (5), using the augmented Lagrangian technique [14]. The final objective function now becomes

$$J(W_1, W_2, Z) = \min_{W_1, W_2, Z} \|X^{tr} - W_2 Z\|_2^2 \\ + \lambda \left\| Z - \phi(W_1 \tilde{X}^{tr}) \right\|_2^2 \quad (6)$$

Here, λ is the regularization parameter that controls the equality between the proxy and latent variable $\phi(W_1 \tilde{X}^{tr})$. To solve (6), we break it into smaller sub problems using alternating direction method of multiplier (ADMM). The sub problems are as follows.

Problem1:

$$\min_{W_1} \left\| \phi^{-1} Z - W_1 \tilde{X}^{tr} \right\|_2^2 \quad (7)$$

Problem2:

$$\min_{W_2} \|X^{tr} - W_2 Z\|_2^2 \quad (8)$$

Problem3:

$$\begin{aligned} & \min_Z \|X^{tr} - W_2 Z\|_2^2 + \lambda \left\| Z - \phi(W_1 \tilde{X}^{tr}) \right\|_2^2 \\ & = \min_Z \left\| \begin{pmatrix} X^{tr} \\ \sqrt{\lambda} \phi(W_1 \tilde{X}^{tr}) \end{pmatrix} - \begin{pmatrix} W_2 \\ \sqrt{\lambda} I \end{pmatrix} Z \right\|_2^2 \end{aligned} \quad (9)$$

All the sub problems are simple least squares problem which have a closed form solution [15]. Once the network is trained, we use weight matrices W_1 and W_2 to obtain a denoised version \hat{X}^{test} of the corrupted test data \tilde{X}^{test} , using (10).

$$\hat{X}^{test} = W_2 \phi(W_1 \tilde{X}^{test}) \quad (10)$$

We compute the denoising error between X^{test} and \hat{X}^{test} using the normalized mean square error (NMSE) shown in (11).

$$NMSE = \frac{\|X^{test} - \hat{X}^{test}\|_2^2}{\|X^{test}\|_2^2} \quad (11)$$

III. DENOISING OF CORRUPTED SIMULATED NARROWBAND DOPPLER-DOA IMAGES

Wall propagation effects on radar signatures have been previously studied using finite difference time domain techniques (FDTD). However, in the prior work [16], a deterministic model of the wall propagation was used. In this paper, we simulated time varying radar returns using two-dimensional stochastic FDTD (sFDTD) technique [13]. The sFDTD method is identical to the traditional FDTD except for the addition of variance equations while updating the electric and magnetic field at each time instant of the finite grid during the leap frog computations. The stochastic model enables us to perform a realistic study of the diversity in the wall propagation effects due to the variations in the wall characteristics. We consider three dielectric walls. The mean and standard deviation of the dielectric constant of the walls are 4 and 10% respectively. The first wall is a homogeneous wall, the second wall is reinforced with metal rods while the third consists of air gaps.

As seen in Fig.2(a), our simulation space extends from -1m to 1m and 0m to 4m along the X and Y directions respectively. The grid size is $1/20^{th}$ the wavelength of the excitation source and the time step is chosen to satisfy Courant stability conditions. The simulation space is bounded by a perfectly matched layer. Each of the walls is 2m wide (along X) and 0.3m thick (Y : 1m to 1.3m) in our setup. We also consider a free space scenario for comparison purposes. The sFDTD simulation is excited by a sinusoidal source transmitting at a center frequency of 7.5GHz for a duration of 36 ns. Independent sFDTD simulations for free space and each of the through-wall conditions are carried out for 10 source positions (\vec{r}_s) as indicated in the figure. These source positions are spaced half-wavelength apart along the X dimension. Multiple sources are used to simulate the radar returns for a ten-element linear array. The sFDTD simulation provides

the mean ($\mu_E(\vec{r}_p, \vec{r}_s)$) and variance ($\sigma_E^2(\vec{r}_p, \vec{r}_s)$) of the time-domain electric field values for every point in the simulation space (\vec{r}_p). We obtain the corresponding frequency domain values using Fourier transform. We consider three point targets moving with radial velocities of -2 m/s, $+2$ m/s and -2 m/s from initial positions of radial distance of 3 m and direction-of-arrivals (DOA) of -22.5° , 0° and 22.5° respectively. A stochastic distribution of electric field values is estimated from every $\mu_E(\vec{r}_p, \vec{r}_s)$ and $\sigma_E^2(\vec{r}_p, \vec{r}_s)$ as shown below

$$E(\vec{r}_p, \vec{r}_s) = \frac{1}{\sqrt{2\pi(\sigma_E^2)}} e^{-\frac{(E-\mu_E)^2}{2\sigma_E^2}} \quad (12)$$

We convolve each value obtained from the stochastic distributions with a two-dimensional point spread function ($h(f_D, \theta)$) - along time and space to obtain a Doppler-azimuth image of one or more targets, $\chi(f_D, \theta)$.

$$\chi(f_D, \theta) = dE(\vec{r}_p, \vec{r}_s) * h(f_D, \theta) \quad (13)$$

The point spread function is a product of two sinc functions. Its width along the Doppler and DOA dimensions are determined by the dwell time of the radar data and the array aperture size.

A. Simulation Results

We generated a total of 200 Doppler-DOA images each of size $[31 \times 181]$, for each wall type and corresponding free space images. These images are vectorised for final processing. The size of the total data set is $[5611 \times 200]$. Of these, 150 images are used for training the autoencoder and the remaining for testing. We set the dimension of the hidden layer to be 50. Weight matrices W_1 and W_2 of sizes $[50 \times 5611]$ and $[5611 \times 50]$ respectively, are initialized randomly. Then we iteratively update them by solving equation (6), using ADMM technique described in the theory section. λ was chosen to be 1. We represent our denoising results using NMSE, defined in 11. The algorithm is run in MATLAB 2015b on an Intel(R) Core(TM) i7-5500U CPU running at 2.40 GHz; 16-GB RAM, Windows 10 (64 b). The results are presented in Table.I. We observe the NMSE(GT) between free space image and different wall types. The high error in the reinforced wall case is due to the significant phase distortions introduced by the metal rods. After denoising, the NMSE(Pred) dropped significantly for all the wall types. Similar observations can be drawn from the images shown in Fig.3. Fig.3(a) shows the Doppler-DOA image of the three moving targets in free space. This image is considered to be the ground truth for our simulations.

The results in Figs.3(b)-(d) show images of the targets in one set of through-wall conditions. We are able to observe distortion in these images due to multipath. Figs.3(e)-(f) show the reconstructed images after they are passed through the denoising autoencoder. We observe that these reconstructed images look very similar to the ground truth in Fig.3(a).

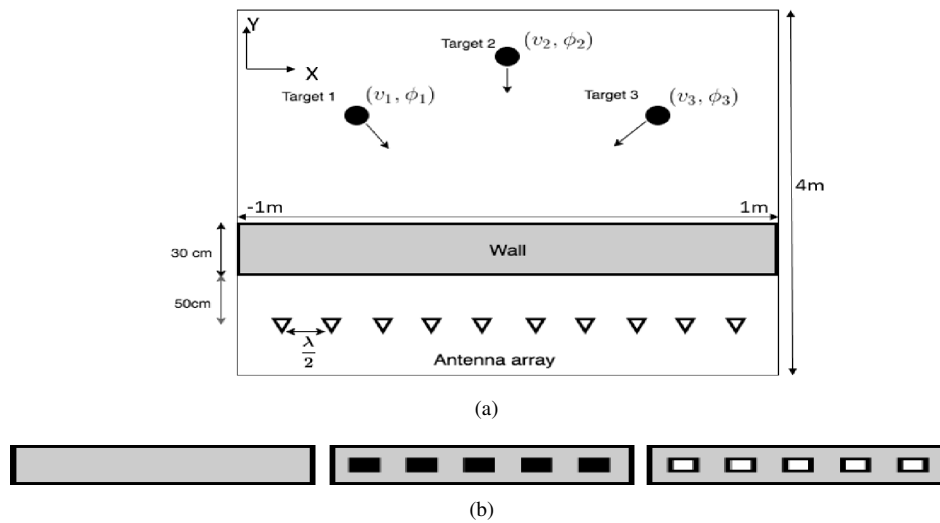


Fig. 2: Simulation setup for stochastic FDTD - (a) the room Geometry and the (b) different wall types (Left- Homogeneous, Centre- Reinforced , Right- Wall with air-gaps).

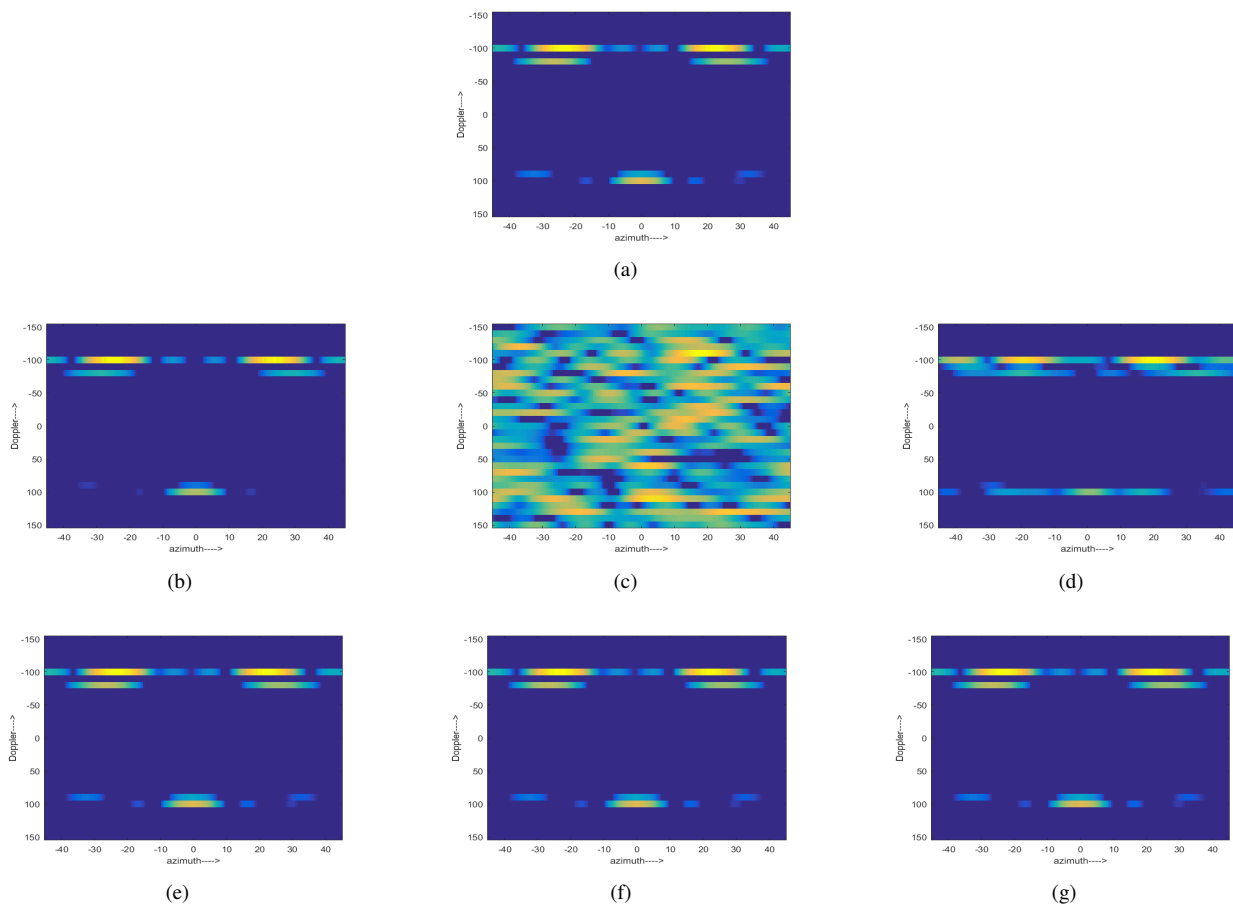


Fig. 3: Simulated Doppler-DOA image of three point scatterers in (a) free space (b) through homogeneous wall, (c) reinforced dielectric wall, (d) dielectric wall with air gaps. Denoised images corresponding to (e) homogeneous wall, (f) reinforced dielectric wall and (g) dielectric wall with air gaps.

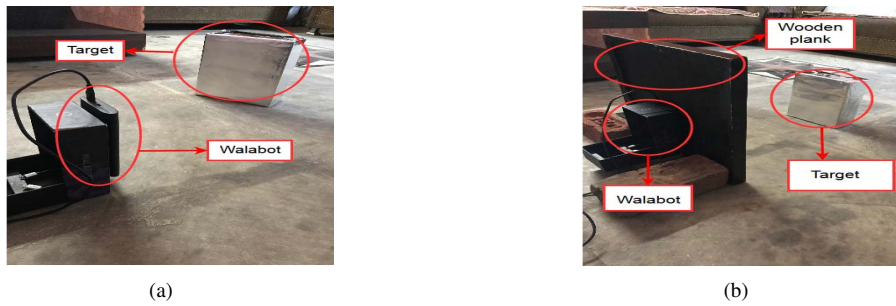


Fig. 4: Measurement setup of frontal imaging by Walabot in (a) line-of-sight (b) through a wooden wall scenarios.

TABLE I: NMSE between target in clean and corrupted images for different through-wall conditions. NMSE (GT):between corrupted image and free space image and NMSE (predicted):between denoised image and free space image

Dielectric	NMSE (GT)	NMSE (predicted)
Homogeneous	2.23	3.2×10^{-4}
Reinforced	56.81	0.02
Wall with Air-gaps	4.76	0.002

IV. DENOISING CORRUPTED FRONTAL IMAGES GENERATED FROM MEASUREMENT DATA IN THROUGH-WALL CONDITIONS

Next, we test the autoencoder algorithm on wideband measurement data collected in through-wall conditions using an RF imaging sensor called the Walabot Pro [17]. In this case, we obtain frontal images by processing wideband data (3.3 - 10.3GHz) from a 4×4 element planar antenna array. The Walabot is an un-calibrated low power sensor which has limited range especially in through-wall conditions. The target is a flat metallic plate of $15\text{cm} \times 20\text{cm}$ dimensions. The experimental data are collected in four scenarios - line-of-sight and through a 1cm thick glass wall and two wooden walls of 2cm and 3.5 cm thicknesses as shown in Fig.4 for multiple locations and orientations of the target with respect to the sensor. We collected 140 different measurements for each scenario. We increased this data set to 250 by introducing random repetition of some cases. We split the measurement data into 200 training images and 50 test images where the size of each image is $[31 \times 31]$. We trained the autoencoder with the clean line-of-sight images and the corresponding corrupted images in through-wall conditions. Once trained, we used the autoencoder to denoise the remaining corrupted through-wall images to reconstruct clean images similar to those obtained under line-of-sight conditions. The algorithms are run in MATLAB 2015b on an Intel(R) Core(TM) i7-5500U CPU running at 2.40 GHz; 16-GB RAM, Windows 10 (64 b). Fig.5 shows the results for one case of the through-glass wall data. Fig.5a is the ground truth or clean image of the target in line-of-sight conditions. This image is distorted due to the interference introduced by the wall as shown in Fig.5b. The distortion is mostly due to the multipath and attenuation introduced by the wall. The reconstructed images, obtained from the denoising

TABLE II: NMSE between target in free space and other dielectrics for different number of nodes (r) in the hidden layers of denoising autoencoder

Dielectric/r	100	200	300	500
Glass	3.9	0.58	0.015	6.5×10^{-4}
Wood (2cm)	8.05	8.36	0.06	0.05
Wood (3.5cm)	3.36	0.06	0.06	9.13×10^{-7}

autoencoder are shown in Fig.5c-e for three different dimensions of the hidden layer of the autoencoder - $R= 100,200$ and 300. We observe that by increasing the dimensionality of the hidden layer in the denoising autoencoder, there is a corresponding improvement in the shape and features extracted image. Table II contains the NMSE between the radar images in through-wall conditions with the corresponding images in line-of-sight conditions as a function of the dimensionality of the hidden layer. The NMSE in all three cases decreases as we increase the dimension of the hidden layer. This is because the hidden layer determines the extent of compression and consequently, the loss of information of the input data. The increased dimensionality (r), however, comes at the price of increased computational complexity which is clearly reflected in Fig.6. The higher error is observed in the case of the 2cm wooden wall. This could be due to multiple reasons - greater in-homogeneity in the 2cm thick wall, the moisture content or the species of wood used may have adversely affected our results.

V. CONCLUSION

We demonstrated the effectiveness of using denoising autoencoders for mitigating through wall interference in both narrowband (Doppler-DOA) and wideband (frontal) radar data. The performance of the algorithm is determined by the in-homogeneity in the wall as well as the dimensionality of the hidden layer of the autoencoder. The algorithm requires no prior information of the wall parameters or analytic model of the through-wall propagation. Instead, the algorithm relies on the availability of large training databases of corrupted and clean radar images. To evaluate the performance of the proposed algorithm in more realistic and difficult scenarios, we propose to test it using both the simulated and measured frontal images of humans, generated using three dimensional

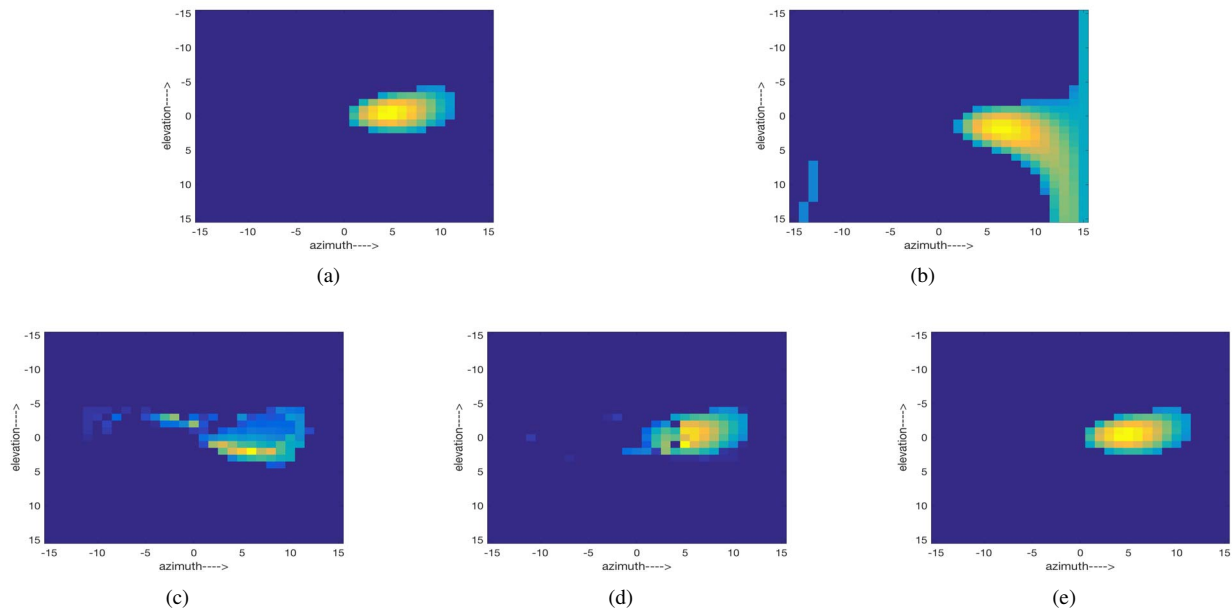


Fig. 5: Radar images (a) in line-of-sight, (b) reconstructed after through wall interference (c,d,e) reconstructed after using denoising autoencoder with dimensions $r_1=100$, $r_2=200$ and $r_3=300$ respectively.

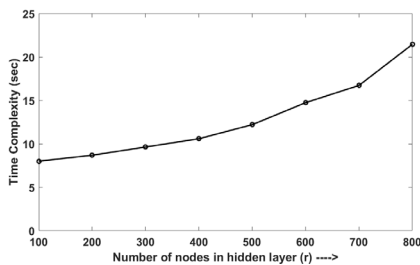


Fig. 6: Variation of training computational time with number of nodes (r) in the hidden layer.

Fourier processing along azimuth, elevation and Doppler in both line of sight and non line of sight conditions. The stochastic model enables us to perform a realistic study of the diversity in the wall propagation effects due to the variations in the wall characteristics.

REFERENCES

- [1] M. G. Amin, *Through-the-wall radar imaging*. CRC press, 2016.
- [2] R. M. Narayanan, M. C. Shastry, P.-H. Chen, and M. Levi, "Through-the-wall detection of stationary human targets using doppler radar," *Progress In Electromagnetics Research B*, vol. 20, pp. 147–166, 2010.
- [3] Y. Jia, G. Cui, L. Kong, and X. Yang, "Multichannel and multiview imaging approach to building layout determination of through-wall radar," *IEEE Geoscience and Remote Sensing Letters*, vol. 11, no. 5, pp. 970–974, 2014.
- [4] C. Clemente, A. Balleri, K. Woodbridge, and J. J. Soraghan, "Developments in target micro-doppler signatures analysis: radar imaging, ultrasound and through-the-wall radar," *EURASIP Journal on Advances in Signal Processing*, vol. 2013, no. 1, p. 47, 2013.
- [5] S. S. Ram, Y. Li, A. Lin, and H. Ling, "Doppler-based detection and tracking of humans in indoor environments," *Journal of the Franklin Institute*, vol. 345, no. 6, pp. 679–699, 2008.
- [6] F. Ahmad, M. G. Amin, and G. Mandapati, "Autofocusing of through-the-wall radar imagery under unknown wall characteristics," *IEEE transactions on image processing*, vol. 16, no. 7, pp. 1785–1795, 2007.
- [7] X. Chen and W. Chen, "Multipath ghost elimination for through-wall radar imaging," *IET Radar, Sonar & Navigation*, vol. 10, no. 2, pp. 299–310, 2016.
- [8] Q. Tan, H. Leung, Y. Song, and T. Wang, "Multipath ghost suppression for through-the-wall radar," *IEEE Transactions on Aerospace and Electronic Systems*, vol. 50, no. 3, pp. 2284–2292, 2014.
- [9] M. Leigsnering, F. Ahmad, M. Amin, and A. Zoubir, "Multipath exploitation in through-the-wall radar imaging using sparse reconstruction," *IEEE Transactions on Aerospace and Electronic Systems*, vol. 50, no. 2, pp. 920–939, 2014.
- [10] G. Cui, L. Kong, and J. Yang, "A back-projection algorithm to stepped-frequency synthetic aperture through-the-wall radar imaging," in *Synthetic Aperture Radar, 2007. APSAR 2007. 1st Asian and Pacific Conference on*. IEEE, 2007, pp. 123–126.
- [11] P. Vincent, H. Larochelle, Y. Bengio, and P.-A. Manzagol, "Extracting and composing robust features with denoising autoencoders," in *Proceedings of the 25th international conference on Machine learning*. ACM, 2008, pp. 1096–1103.
- [12] S. Boyd, N. Parikh, E. Chu, B. Peleato, and J. Eckstein, "Distributed optimization and statistical learning via the alternating direction method of multipliers," *Foundations and Trends® in Machine Learning*, vol. 3, no. 1, pp. 1–122, 2011.
- [13] S. M. Smith and C. Furse, "Stochastic ftdt for analysis of statistical variation in electromagnetic fields," *IEEE Transactions on Antennas and Propagation*, vol. 60, no. 7, pp. 3343–3350, 2012.
- [14] D. P. Bertsekas, *Nonlinear programming*. Athena scientific Belmont, 1999.
- [15] C. M. Bishop, "Pattern recognition," *Machine Learning*, vol. 128, pp. 1–58, 2006.
- [16] S. S. Ram, C. Christianson, Y. Kim, and H. Ling, "Simulation and analysis of human micro-dopplers in through-wall environments," *IEEE Transactions on Geoscience and remote sensing*, vol. 48, no. 4, pp. 2015–2023, 2010.
- [17] 2017. [Online]. Available: <https://walabot.com/docs/walabot-tech-brief-416.pdf>